Modelling and control of an autonomous articulated mining vehicle navigating a predefined path

B.J. Alshaer*, T.T. Darabseh and A.Q. Momani

Department of Mechanical Engineering,
Jordan University of Science and Technology,
Irbid 22110, Jordan
E-mail: bjalshaer@just.edu.jo
E-mail: darabseh@just.edu.jo E-mail: alshabj@just.edu.jo
*Corresponding author

Abstract: This research is conducted on machine dynamics and steering control of an articulated surface mining large wheel loader (LWL) navigating a predefined path. Modelling a LWL based on computational multibody dynamics is achieved by modelling each system of the articulated vehicle separately then merging them to form an overall system of an articulated vehicle navigating a predefined path. This model includes the front and rear frames, articulated hinge, steering actuators, tyre model, steering controller and a predefined path. Fuzzy and PID steering controllers are developed and simulated. Results show that it is possible to model large articulated vehicles as a multibody mechanical system. Both of the developed controllers are able to control the lateral and longitudinal motion of the vehicle and drive the machine over the desired path accurately. The fuzzy logic controller has longer rising time but shorter settling time when compared with the PID controller.

Keywords: articulated vehicle; automated vehicle; vehicle modelling; steering control; wheel loader; tyre model.

Reference to this paper should be made as follows: Alshaer, B.J., Darabseh, T.T. and Momani, A.Q. (2014) 'Modelling and control of an autonomous articulated mining vehicle navigating a predefined path', *Int. J. Heavy Vehicle Systems*, Vol. 21, No. 2, pp.152–168.

Biographical notes: Bassam J. Alshaer received his BSc and MSc from Jordan University of Science and Technology in 1991, and 1994, respectively. He received his PhD in Mechanical Engineering from Wichita State University, USA, in 2000. His current research interests include multi-body dynamics, modeling and simulation of heavy construction machines, heavy construction machines systems and technology, autonomous systems.

Tariq T. Darabseh obtained his BSc and MSc from Jordan University of Science and Technology in 1992, and 1994, respectively. He received his PhD in Mechanical Engineering from New Mexico State University, USA, in 2002. His current research interests are dynamic stability, finite elements analysis, and thermal stresses.

Ahmad Q. Momani obtained his BSc and MSc from Jordan University of Science and Technology in 2006 and 2011, respectively. His current research interests are mechatronic systems, artificial intelligent and robotics.

1 Introduction

The environment of articulated vehicles workspace is usually hazardous with many blind spots where the possibilities of operator injury is high, so the need for automation appears for safety and keeping high productivity. Automated articulated vehicle work cycle has recently received considerable attention with many applications such as automated mines and construction sites. Articulated mining large wheel loaders (LWLs) can be divided into two main categories; underground and surface mining loaders. The underground mining loaders such as the load-haul-dump loaders (LHD) are smaller in size compared to those used in surface mining such as LWL. Although there is a wealth of literature on underground mining LHD wheel loaders, the vehicles that operate overground have received less attention due to their size and open workspace path shape variation.

The LWL shown in Figure 1 is a four wheeled articulated vehicle whose steering is done by controlling the angle of the pivot joint between the front and rear bodies using a hydraulic system and hydraulic actuators connecting the two main frames of the wheel loader. Each body is equipped with a single axle with non-steerable wheels, wheel loaders usually used to load many kinds of materials into another type of machinery such as trucks. The machine under consideration is a typical LWL similar to Caterpillar 994F or Volvo L350F. A lot of research has been conducted trying to model, simulate and control articulated vehicles with focus on explaining the nature of their dynamic response, few of these researches focused on the surface mining and constructions wheel loaders. Koyachi and Sarata (2009) developed a real sized autonomous wheel loader and succeeded to execute the unmanned and autonomous task including path following control, the wheel loader they considered was 'Yamazumi-4' which weighs less than 7 tons. Ghabcheloo and Hyvönen (2009) addressed the problem of autonomous steering of a hydraulically actuated articulated-frame-steering wheel loader, their kinematic model is derived under simplifying assumptions such as no slipping and no skidding, and their test platform is a small prototype wheel loader based on Avant 635. Debeleac (2009) proposed a methodology capable to simulate the nonlinear behaviour of interaction between a small size wheel loader and uneven terrain, the study deals with nonlinear approaches in dynamic behaviour analysis for multibody mechanical systems by using advanced computing and simulation tools, the model used is unarticulated drive earthmoving wheel loader. Filla (2005) developed an event-driven controller model for dynamic simulation of construction wheel loaders; the operator model presented focuses on a short loading V-shape cycle and uses a pure discrete-event approach instead of full PID or Fuzzy controller, this results in one entity model contains vehicle, path and an operator, i.e., changing any of these component such as path shape leads to a need to update the other two components. Norris et al. (2006) implemented a dynamic model of an articulated off-road wheel loader to determine the vehicle steering manoeuvrability via real-time simulation, the model they used is simplified to containing only the necessary details of the vehicle turning dynamics to make the real-time virtual simulation goal accomplished. Sarata et al. (2006) developed autonomous system for loading operation by a wheel loader; however the focus of their work is on loading the bucket from the pile, they limited their work to V-shape paths. Alshaer et al. (2013) presented a virtual model of a heavy articulated work machine

conducting a loading cycle, however their focus is path planning and they limited their work to V-shape only.

Figure 1 Lateral view of a large wheel loader

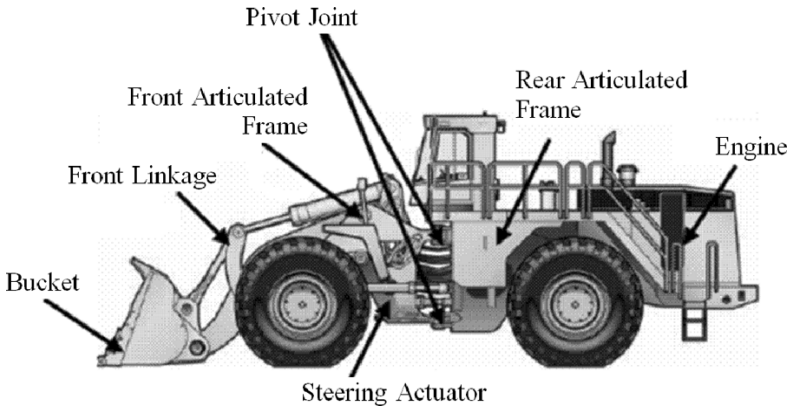

LHD mining loaders received a considerable attention in literature (Ridley and Corke, 2001; Corke and Ridley, 2001; DeSantis, 1997; Altafini, 1999; Dragt et al., 2005; Yavin, 2005; Sarata et al., 2005a, 2005b, 2008; Yossawee et al., 2002; Ho et al., 2003; Lamiraux et al., 2003; Divelbiss and Wen, 1997; Ghabcheloo et al., 2009; Sasiadek and Lu, 2005; Polotski and Hemami, 1997; Ferrara and Magnani, 2004; Kalyoncu, 2007) compared to surface mining LWL, there are basic differences between these two types of loaders based on size and operational path specifications. LHD underground loaders navigate a well defined invariable smooth path through a tunnel, usually marked with lines and sensors, which facilitates automating such machines. LWLs navigating above-ground in an open workspace have paths that vary with every cycle based on terrain, dump-truck location and pile shape variation due to scooping. LWLs weight is usually more than twice the weight of LHD loader. These differences make it harder to control LWL to navigate a predefined path.

2 Scope and objectives of the research

A methodology is proposed in this research to model and simulate an articulated LWL navigating a predefined path based on computational multibody dynamics. The front and rear frames are modelled as two rigid bodies in planar motion with revolute joint constraint. The tyres are modelled as forces acting on wheel centre, these forces are delivered from enhanced tyre model, the enhanced tyre model calculates the resulted forces and torques from the interaction between tyres and road based on machine's velocity and position. Steering actuator is modelled as kinematic constraint acting on revolute pivot between front and rear frames. Fuzzy logic and PID are developed and applied. Using the proposed formulation and control, the performance of the articulated vehicle to follow a certain path is predicted and evaluated. In general, this research is expected to be of great use in the analysis of path tracking problems and automated working sites researches where the desired path is predefined during a loading cycle and varies from one cycle to another.

3 Modelling the multibody mechanical system of an articulated large wheel loader

3.1 Desired path and feedback errors specifications

Reeds and Shepp (1990) proposed an algorithm to determine the optimal path between two points. Their algorithm simply gives a set of paths which contains arcs and straight segments, the segments could be in forward or reverse direction. Figure 2 shows an example of what Reed and Shepp proposed. In this work, two different paths are utilised to conduct the simulations and virtual testing. The vehicle first is simulated while navigating a circular path, then a path with variable segments based on Reeds and Shepp methods is developed and used. These two paths are plotted in the results' section along with the results' plots. Due to the fact that any complex paths can be approximated to a set of joined circular and linear segments (Reeds and Shepp, 1990), then whatever applied on these two paths can be extended to more complex paths.

Figure 2 Optimal paths possibilities for a point that has the same starting and target points but with opposite orientation

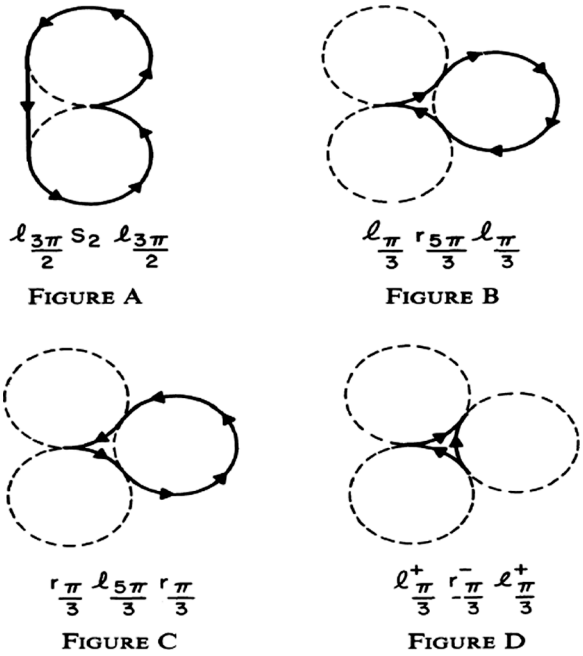

Source: Reeds and Shepp (1990)

The focus of this paper is not the specific ground-tyre interaction, so the vehicle is assumed driving over a flat level road surface along the specifed paths. For controlling purposes and to represent the deviation of the machine from the desired location; three errors are introduced as shown in Figure 3, displacement error (E_d), heading error (E_h) and curvature error (E_c). Displacement error is calculated by extending the line that connects front axle midpoint and actual path centre to intersect with the desired path, the distance between intersection point and front axle midpoint called displacement error, displacement error is positive when intersection point lies on the positive y-axis of the

vehicle local coordinate system and negative otherwise. Point C_d is the desired path centre, while point C_a represents the actual path centre, the heading error (E_h) is the angle formed when connecting these two points to the front axle midpoint, the heading error is calculated using dot product. Curvature error is the difference between vehicle curvature (actual path) and desired circular path curvature which can be presented using the equation $E_c = 1/r - 1/R$, where r is instantaneous radius of rotation for the vehicle (radius of the actual path) and R is the radius of the desired path.

Figure 3 Controller feedback errors definition

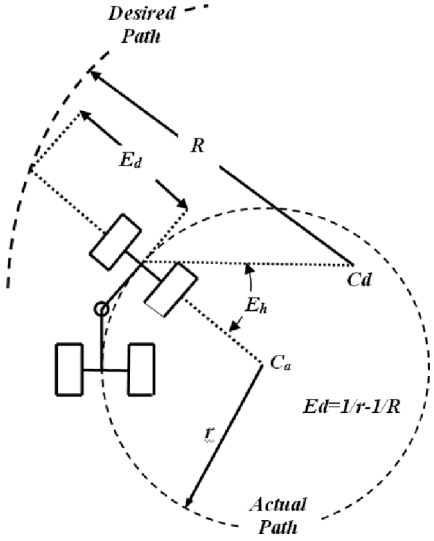

3.2 Controller setup

Figure 4 shows the steering controller setup used to control the vehicle, the controller uses the machine actual location compared with the predefined path to calculate the required feedback errors. Two different controllers are developed and used as discussed next.

Figure 4 Steering control loop

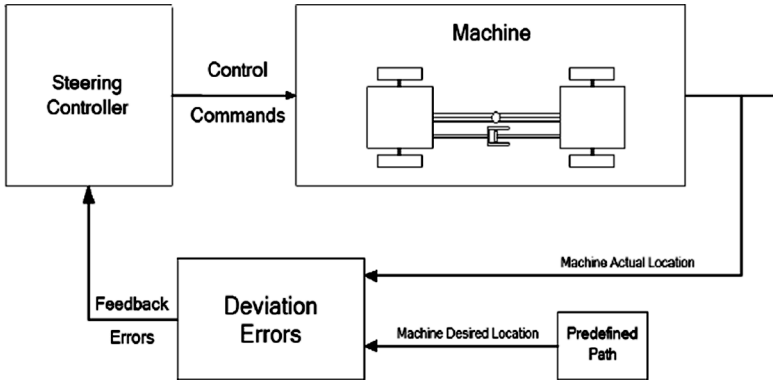

3.2.1 PID steering control

A PID controller is developed and used to control the actual path of the vehicle. The machine actual location compared with predefined path to calculate the feedback errors which required by the controller, then each error entered to a separate PID controller, the results are summed together to make one of the control outputs which is the steering command as shown in Figure 5. Steering speed is limited by the vehicle capabilities; mainly the machine dynamic lateral stability, operator comfort, and steering actuator force limit. The PID controller also controls the machine speed based on the curvature error, whenever the curvature error is small then go fast, otherwise slow down the vehicle to help in correcting the actual path of the vehicle. The PID controller parameters are shown in Figure 5.

Figure 5 PID controller layout and parameters

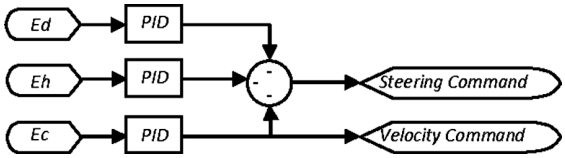

3.2.2 Fuzzy logic steering control

A fuzzy controller which has three inputs and two outputs is developed and used in this research. The controller inputs are displacement, heading and curvature errors, while the outputs are steering speed (degrees/s) and vehicle speed as a percentage of the maximum speed. The fuzzy controller rules which regulate the relationships between the inputs and the outputs are shown in Figure 5, E_d stands for displacement error, E_h for heading error, E_c for curvature error, N for negative, Z for zero and P for positive.

Figure 6 Fuzzy logic controller memberships for inputs and outputs

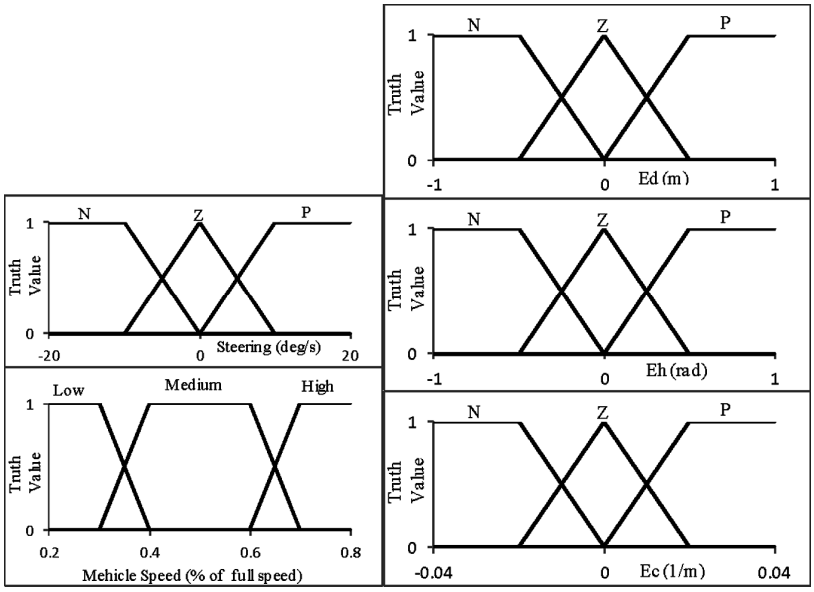

3.3 Main frames modelling

In modelling a multibody mechanical system; the links and bodies may be interconnected by one or more kinematic joints. Figure 7 represents a wheel loader which consists of two frames connected by a revolute joint located at point *P*. Bodies *i* and *j* represent the rear and front frames respectively. *XY* is the fixed global coordinate system. $\xi\eta$ is the local coordinate systems which are attached and fixed to the bodies, the origins of the local coordinate systems of bodies *i* and *j* are located at (X_i, Y_i) and (X_j, Y_j) respectively and they are rotated at arbitrary angles ϕ_i and ϕ_j respectively. The vector of coordinates for bodies *i* and *j* is:

$$\boldsymbol{q} = [X_i, Y_i, \phi_i, X_j, Y_j, \phi_j]^T \tag{1}$$

The kinematic joints can be described as algebraic constraint equations. The front and rear bodies in an articulated vehicle modelling are connected together by revolute joint which is lower-pair kinematic joint that does not need any information on the shape of the connected bodies.

Figure 7 Global and local coordinates for a multibody mechanical system of a wheel loader

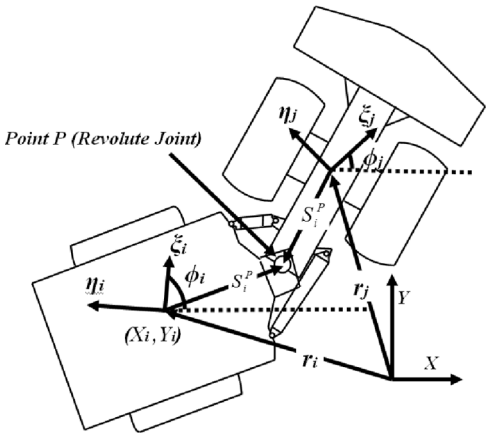

The revolute joint located at point *P* in Figure 7 can be located from the origin of the $\xi_i\eta_i$ axes by the vector $\boldsymbol{s}_i^P$, and from the origin of the $\xi_j\eta_j$ axes by the vector $\boldsymbol{s}_i^P$. From the loop vectors we can write

$$\boldsymbol{r}_i + \boldsymbol{s}_i^P - \boldsymbol{r}_j - \boldsymbol{s}_j^P = 0$$

where $\boldsymbol{r}_i$ and $\boldsymbol{r}_j$ are the origins of bodies *i* and *j* respectively, the previous equation which represents the constraints imposed by the revolute joint can be expressed as:

$$\boldsymbol{\Phi}(\boldsymbol{q}) = [\boldsymbol{0}] \tag{2}$$

or in an expanded form as:

$$X_i + \xi_i^P \cos\phi_i - \eta_i^P \sin\phi_i - X_j - \xi_j^P \cos\phi_j + \eta_j^P \sin\phi_j = 0 \tag{3}$$

$$Y_i + \xi_i^P \sin\phi_i + \eta_i^P \cos\phi_i - Y_j - \xi_j^P \sin\phi_j - \eta_j^P \cos\phi_j = 0 \tag{4}$$

where (ξ_i^P, η_i^P) and (ξ_j^P, η_j^P) are the revolute joint local coordinates with respect to local coordinates $\xi\eta$ of bodies *i* and *j* respectively.

The dynamic equations of motion that rule the behaviour of a constraint multibody mechanical system in general are

$$\boldsymbol{M}\ddot{\boldsymbol{q}} - \boldsymbol{\Phi}_{\boldsymbol{q}}^{\boldsymbol{T}}\boldsymbol{\lambda} = \boldsymbol{g} \tag{5}$$

where $\boldsymbol{M}$ is the mass matrix shown in expanded form in equation (8), $\boldsymbol{q}$ is the system coordinate vector shown in equation (1), $\boldsymbol{\Phi}_{\boldsymbol{q}}$ the Jacobian matrix (derived from the constraint equations), $\boldsymbol{\lambda}$ is vector of Lagrange multipliers (reaction forces), and $\boldsymbol{g}$ is the total forces acting on the system (both external and constraint forces). To put equation (5) in expanded form we need to evaluate $\boldsymbol{\Phi}_{\boldsymbol{q}}$ and $\boldsymbol{g}$ the Jacobian matrix $\boldsymbol{\Phi}_{\boldsymbol{q}}$ can be evaluated by differentiating equations (3) and (4) with respect to vector $\boldsymbol{q}$ (which is defined in equation (1)), doing so yields:

$$\boldsymbol{\Phi}_{\boldsymbol{q}}^{T} = \begin{bmatrix} 1 & 0 & d_{ri}\sin\phi_i & -1 & 0 & d_{rj}\sin\phi_j \\ 0 & 1 & d_{ri}\cos\phi_i & 0 & -1 & d_{rj}\cos\phi_j \end{bmatrix} \tag{6}$$

where in equation (6); the distances d_{ri} and d_{rj} represent the location of the revolute joint (point *p*) with respect to the local coordinate system as shown in Figure 8.

Figure 8 Free body diagram of body I showing external forces and reactions

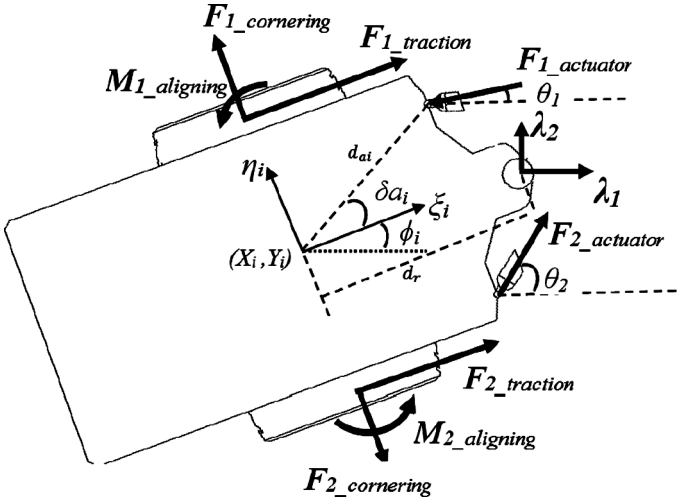

To evaluate the external forces vector $\boldsymbol{g}$ in equation (5), Figure 8 shows the free body diagram for the rear frame of the wheel loader, i.e., body *i*. The local coordinate system $\xi\eta$ is taken such that the origin (X_i, Y_i) lies on the middle of the axle and is oriented in a way that η_i is along the axle, in this way the angle of rotation of local coordinate system ϕ_i is actually the same as the yaw angle of the body. The Lagrange multipliers represent the constraints (reaction forces) produced by the revolute joints. The rest of the external forces affecting the rear frame are shown on the free body diagram in Figure 8, these external forces come from the tyres and the actuators. Body *j* has similar external forces and same reaction forces with opposite directions. Taking into

consideration these forces; the total forces acting on the system (***g***) in equation (5) can be written as:

$$\begin{bmatrix} f_{Xi} \\ f_{Yi} \\ n_i \\ f_{Xj} \\ f_{Yj} \\ n_j \end{bmatrix} = \begin{bmatrix} (F_{1i\_tr} + F_{2i\_tr})\cos\phi_i + (-F_{1i\_cor} + F_{2i\_cor})\sin\phi_i - F_{1\_act}\cos\theta_1 + F_{2\_act}\cos\theta_2 \\ (F_{1i\_tr} - F_{2i\_tr})\sin\phi_i + (F_{1i\_cor} - F_{2i\_cor})\cos\phi_i - F_{1\_act}\sin\theta_1 + F_{2\_act}\sin\theta_2 \\ (-F_{1i_{tr}} + F_{2i_{tr}})d_{i_{tr}} + F_{1_{act}}(-d_{axi}\sin\theta_1 + d_{ayi}\cos\theta_1) + F_{2_{act}}(d_{axi}\sin\theta_2 + d_{ayi}\cos\theta_2) \\ (F_{1j_{tr}} + F_{2j_{tr}})\cos\phi_j + (-F_{1j_{cor}} + F_{2j_{cor}})\sin\phi_j + F_{1_{act}}\cos\theta_1 - F_{2\_act}\cos\theta_2 \\ (F_{1j\_tr} - F_{2j\_tr})\sin\phi_j + (-F_{1j_{cor}} - F_{2j_{cor}})\cos\phi_j + F_{1\_act}\sin\theta_1 - F_{2\_act}\sin\theta_2 \\ (-F_{1i_{tr}} + F_{2i_{tr}})d_{i_{tr}} - F_{1_{act}}(-d_{axi}\sin\theta_1 + d_{ayi}\cos\theta_1) + F_{2_{act}}(d_{axi}\sin\theta_2 + d_{ayi}\cos\theta_2) \end{bmatrix} \tag{7}$$

and equation (5) can be written in expanded form as:

$$\begin{bmatrix} m_i & 0 & 0 & 0 & 0 & 0 \\ 0 & m_i & 0 & 0 & 0 & 0 \\ 0 & 0 & \mu_i & 0 & 0 & 0 \\ 0 & 0 & 0 & m_j & 0 & 0 \\ 0 & 0 & 0 & 0 & m_j & 0 \\ 0 & 0 & 0 & 0 & 0 & \mu_j \end{bmatrix} \begin{bmatrix} \ddot{X}_i \\ \ddot{Y}_i \\ \ddot{\phi}_i \\ \ddot{X}_j \\ \ddot{Y}_j \\ \ddot{\phi}_j \end{bmatrix} - \begin{bmatrix} 1 & 0 \\ 0 & 1 \\ d_{ri}\sin\phi_j & d_{ri}\cos\phi_i \\ -1 & 0 \\ 0 & -1 \\ d_{rj}\sin\phi_j & d_{rj}\cos\phi_j \end{bmatrix} \begin{bmatrix} \lambda_1 \\ \lambda_2 \end{bmatrix} = \begin{bmatrix} f_{Xi} \\ f_{Yi} \\ n_i \\ f_{Xj} \\ f_{Yj} \\ n_j \end{bmatrix} \tag{8}$$

where in equations (7) and (8):

m_i, m_j: Masses of body i (vehicle's front frame) and body j (Vehicles rear frame) respectively

μ_i, μ_j: Moment of inertia of body i and body j respectively

λ_1, λ_2: Reaction forces in the revolute joint (hitch joint connecting the frames of the vehicle)

f_{Xi}, f_{Yi}: The sum of all forces acting on body i in the X and Y directions respectively

f_{Xj}, f_{Xj}: The sum of all forces acting on body j in the X and Y directions respectively

n_i, n_j: The sum of all moments acting on body i and j respectively

$d_r \sin\phi$, $d_r \cos\phi$: The moments arms for the reactions (λ) as shown in Figure (8).

Moments in equation (7) are evaluated at the origin of the local coordinate systems of the bodies. In equation (7), θ is the actuator angle with reference to the global coordinate system, θ is function of the body yaw angle ϕ, so the external forces in equation (7) are functions of the forces of the tyres, the forces of the actuators, and the bodies' yaw angles ϕ_i and ϕ_j. Also in equation (7), the traction, cornering and actuator forces as well as the aligning moments are known quantities. The evaluation of these forces and moments is discussed next.

3.4 Evaluating actuators forces

A sketch for an actuator connecting the rear frame (body *i*) and the front frame (body *j*) of a wheel loader is shown in Figure 9. a_i and a_j are the points where the actuator is connected to bodies *i* and *j* respectively. The distances s^{ai} and s^{aj} represent the locations of points a_i and a_j respectively. Angles γ_{ai} and γ_{aj} represent the angles that distances s_{ai} and s_{aj} make with the local coordinate systems of body *i* and body *j* respectively. Quantities s^{ai}, s^{aj}, γ_{ai}, and γ_{aj} are constants due to referencing to the local coordinate systems, their values depend on the wheel loader geometry arrangement. The target is to relate the actuator angle (θ_{a1}) to the global coordinate system *XY*. The loop vector analysis shows that

$$\theta_{a1} = \tan^{-1} \frac{s_{aj} \sin(\phi_j + \gamma_{aj}) - s_{ai} \sin(\phi_i + \gamma_{ai})}{s_{aj} \cos(\phi_j + \gamma_{aj}) - s_{ai} \cos(\phi_i + \gamma_{ai})} \tag{9}$$

Due to the geometric symmetry of both actuators over the local coordinate axis ξ, then equation (9) gives θ_{a2} when negative values for γ_{ai} and γ_{aj} are used. The value of the force produced by the actuator depends on the size of the actuator and the produced internal hydraulic pressure, that is $Fact = Pressure \times (Head\ \ Area - Rod\ \ Area)$, the areas are constants. It can be assumed that the pressure has a linear relation with the controller steering signal, which yields:

$$F_{1i_{act}} = Const. \times Steering\ \ Command \tag{10}$$

The actuator is a two force member, i.e., the line of action of the force produced by an actuator is along its extension, this results in $F_{1j_{act}} = -F_{1i_{act}}$, $F_{2i_{act}} = -F_{1i_{act}}$ and $F_{2j_{act}} = -F_{2i_{act}}$.

Figure 9 Front (body *j*) and rear (body *i*) frames connected by a revolute joint and an actuator (see online version for colours)

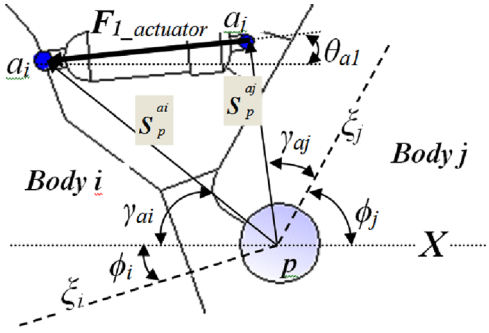

3.5 Evaluating tyres forces

Tyre is one of the most crucial contributor components in modelling the vehicles dynamics. The inputs to the tyre model are the location and orientation of the wheel hub in the global reference frame, the rotational velocity of the wheel in the global frame, and the rotational speed of the drivetrain. The outputs from the tyre model are the forces and moments generated by the tyre's contact with the ground. The contact patch forces

include the traction force (F_x), cornering force (F_y), normal force (F_z) and self-aligning torque (M_z), these quantities are described in Figure 10. (xy) coordinates used here are tyre local coordinates and are not the global coordinate system XY used in Figure 8, in fact x is a tyre local coordinate aligns with ξ body coordinate axis shown in Figure 8 and y aligns with η.

Figure 10 Tyre modelling

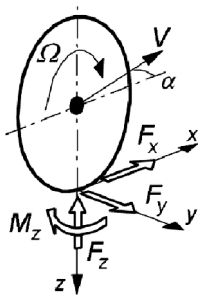

Forces and moment of Figure 10 occur as a result of incompletely symmetric structure of the tyre under loading. Traction force is a function of slip and normal force. While cornering force and self-aligning torque are functions of slip angle and normal force. An equation with empirical coefficients known as the *Pacejka's Magic Formula* (Pacejka, 2002) is used to define the relationship between these quantities. The Magic Formula is an empirical equation that is often used to represent the contact patch forces in the tyre model. The general form of the magic formula is

$$F_x = D_x \sin(C_x \arctan(B_x((1-E_x)\kappa + (E_x / B_x)\arctan(B_x\kappa))) \tag{11}$$

$$F_y = D_y \sin(C_y \arctan(B_y((1-E_y)\alpha + (E_y / B_y)\arctan(B_y\alpha))) \tag{12}$$

$$M_z = D_z \sin(C_z \arctan(B_z((1-E_z)\alpha + (E_z / B_z)\arctan(B_z\alpha))) \tag{13}$$

Each one of these quantities represents a curve where coefficient D is the maximum peak value of the curve, C determines the shape of the curve, B determines the initial slope of the curve and E is the curvature factor that controls location of the peak and the curve curvature. Pacejka magic formula is a function of longitudinal slip κ and the slip angle α in case of a constant normal force F_z. Coefficients D, C, B and E are functions of more than 20 other empirical constant values that vary from one tyre to another. These constants are obtained from a large set of tests designed to measure the tyres response to a variety of combinations of vertical load, slip, slip angle, and camber angle. The friction effect is incorporated in these coefficients as a result of the experimental readings. Consequently, it is decided to utilise in this work a semi-empirical model known as the enhanced non-linear tyre model along with the Pacejka formula (2002).

The enhanced non-linear tyre model (Pacejka, 2002) is utilised to represents the behaviour for each tyre. Figure 11 illustrates the structure of the enhanced transient model. The contact patch can deform in the tangential and lateral directions with respect to the lower part of the wheel rim. Only the circumferential deflection will be considered

in this work for the enhanced tyre model. The equation of motion of the contact patch mass point for the longitudinal components V_{sx}^* is introduced with the mass m_c, the longitudinal tyre's deflection u, the damping ratio k_{cx} and the carcass stiffness c_{cx} as

$$m_c \dot{V}_{sx}^* + k_{cx}\dot{u} + c_{cx}u = F_x(\kappa', \alpha', F_z) \tag{14}$$

Figure 11 Enhanced transient tyre model in top and side view showing carcass compliances

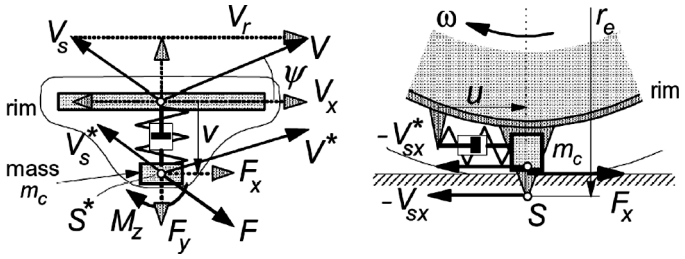

The traction force from the ground to the contact patch F_x is computed from Pacejka's formula. To smooth the progress of calculation near or at the standstill and at the braking conditions, the contact patch relaxation length σ_c is introduced as a part of the differential equation

$$\sigma_c \frac{\mathrm{d}\kappa}{\mathrm{d}t} + |V_x|\,\kappa = -V_{sx}^* \tag{15}$$

where σ_c is the relaxation length (Pacejka, 2002) of the contact patch. The slip κ is obtained from this equation which acts as an input in Pacejka's formula to determine F_x. σ_c value is chosen to be a small but finite value. The slipping velocity (V_s) of the of contact point that is fixed to the wheel body is

$$\boldsymbol{V}_s = \boldsymbol{V} + \frac{re}{r}\boldsymbol{\omega} \times \boldsymbol{r} \tag{16}$$

where r is the loaded tyre radius, r_e is the effective rolling radius and $\boldsymbol{\omega}$ is the angular velocity of the wheel with respect to the inertial frame. The longitudinal carcass stiffness c_{cx} is determined be satisfying the equation

$$\sigma_{\kappa o} = \frac{CF\kappa}{c_{cx}} + \sigma_c \tag{17}$$

where σ_c is the relaxation length and $C_{F\kappa}$ is the longitudinal slip stiffness. The deflection rate in the equation of motion is equal to the difference between the slip velocities of the contact patch and the wheel rim

$$\dot{u} = V_{sx}^* - V_{sx} \tag{18}$$

V_{sx} is the longitudinal component of V_s. The longitudinal force acting on the wheel rim reads

$$F_{xa} = k_{cx}\dot{u} + c_{cx}u \tag{19}$$

The equation of motion of the wheel is governed by

$$m\dot{V}_x = F_{xa} \tag{20}$$

$$I_w\dot{\Omega} = M_D - r_e F_{xa} \tag{21}$$

where I_w wheel's inertia, M_D driving moment, and r_e Effective rolling radius. The linear model is considered to represent the lateral slip. The application considered in this research operates in a combined slip condition. The differential equation for lateral deflection v (Pacejka, 2002) reads

$$\frac{\mathrm{d}v}{\mathrm{d}t} + \frac{1}{\sigma_\alpha}|V_x|v = |V_x|\alpha = -V_{sy} \tag{22}$$

with α is the lateral wheel slip ratio: $\alpha \approx -V_{sy}/|V_x|$. For linear and small slip values

$$\alpha' \approx \tan\alpha' = \frac{v}{\sigma_\alpha}, \quad F_y = C_{F\alpha}\alpha' \tag{23}$$

where C_{Fy} is lateral stiffness of standing tyre, $C_{F\alpha}$ cornering stiffness

4 Numerical solution

Kinematic velocity and acceleration equations are obtained by deriving the constraint equation (2) twice as shown below in equations (24) and (25) respectively:

$$\boldsymbol{\Phi}_q\dot{\boldsymbol{q}} = [0] \tag{24}$$

$$\boldsymbol{\Phi}_q\ddot{\boldsymbol{q}} = [\boldsymbol{\Gamma}] \tag{25}$$

where $\boldsymbol{\Phi q}$ is the Jacobian matrix as shown in equation (6), $\dot{\boldsymbol{q}}$ is the velocity vector (time derivative of equation (1)), and $\ddot{\boldsymbol{q}}$ is the acceleration vector (second time derivative of equation (1)), and vector $\boldsymbol{\Gamma}$(from the derivation) is

$$[\boldsymbol{\Gamma}] = \begin{bmatrix} (d_{ri}\cos\phi_i)\dot{\phi}_i^2 - (d_{rj}\cos\phi_j)\dot{\phi}_j^2 \\ (d_{ri}\sin\phi_i)\dot{\phi}_i^2 - (d_{rj}\sin\phi_j)\dot{\phi}_j^2 \end{bmatrix} \tag{26}$$

d_{ri} is shown in Figure 8, appending equations (5) and equation (25) gives the equations of motion for the multibody system of the articulated vehicle:

$$\begin{bmatrix} \boldsymbol{M} & \boldsymbol{\Phi}_q^T \\ \boldsymbol{\Phi}_q & 0 \end{bmatrix}\begin{bmatrix} \ddot{\boldsymbol{q}} \\ -\boldsymbol{\lambda} \end{bmatrix} = \begin{bmatrix} \boldsymbol{g} \\ \boldsymbol{\Gamma} \end{bmatrix} \tag{27}$$

The Jacobian matrix $\boldsymbol{\Phi q}$ is a function of $\boldsymbol{q}$, vectors $\boldsymbol{g}$ and $\boldsymbol{\Gamma}$ are functions of $\dot{\boldsymbol{q}}, \ddot{\boldsymbol{q}}$ and time (t). Therefore, starting with a valid initial guesses on the position; equations (2) and (24) are solved to find the initial conditions for positions $\boldsymbol{q}$ and velocities $\dot{\boldsymbol{q}}$ at initial time. Then equation (27) provides 8 linear algebraic equations in (8) unknowns that can be solved for $\ddot{\boldsymbol{q}}$ and $\boldsymbol{\lambda}$, afterward, numerical integration of $\dot{\boldsymbol{q}}$ and $\ddot{\boldsymbol{q}}$ yields $\boldsymbol{q}$ and $\dot{\boldsymbol{q}}$ respectively at new time step, and then equation (27) is used again to solve for the $\ddot{\boldsymbol{q}}$ at this new time step.

5 Results and conclusions

Figure 12 shows the simulation results for a 50 ton articulated wheel loader navigating a predefined circular path, the figure shows the desired circular path, the actual path of the the machine, and the controllers feedback errors. Two different controllers to model the human operator steering command have been developed and used in the simulations; the solid lines represent the PID controller results while the dashed lines represent the fuzzy logic controller results. The focus is on modelling the wheel loader as a multibody mechanical system and having the machine model to navigate the desired path. Figure 12 shows that both of the fuzzy logic and the PID controllers drove the machine close to the desired path. Both controllers; the fuzzy logic and the PID, have reasonable rising and settling times. When comparing between the fuzzy logic and PID controllers; the PID controller brought the vehicle faster closer to desired path, however it tooks longer settling time to settle the machine on the desired path compared with the fuzzy logic controller, this can be confirmed when reading the feedback errors plots. Figure 12 also shows the controllers' feedback errors, these feedback variables represent a measure of the machine deviation from the desired path, the machine displaced and disoriented from the desired path, controllers then brought the machine to follow the desired path.

Figure 12 An articulated vehicle navigating a predefined circular path

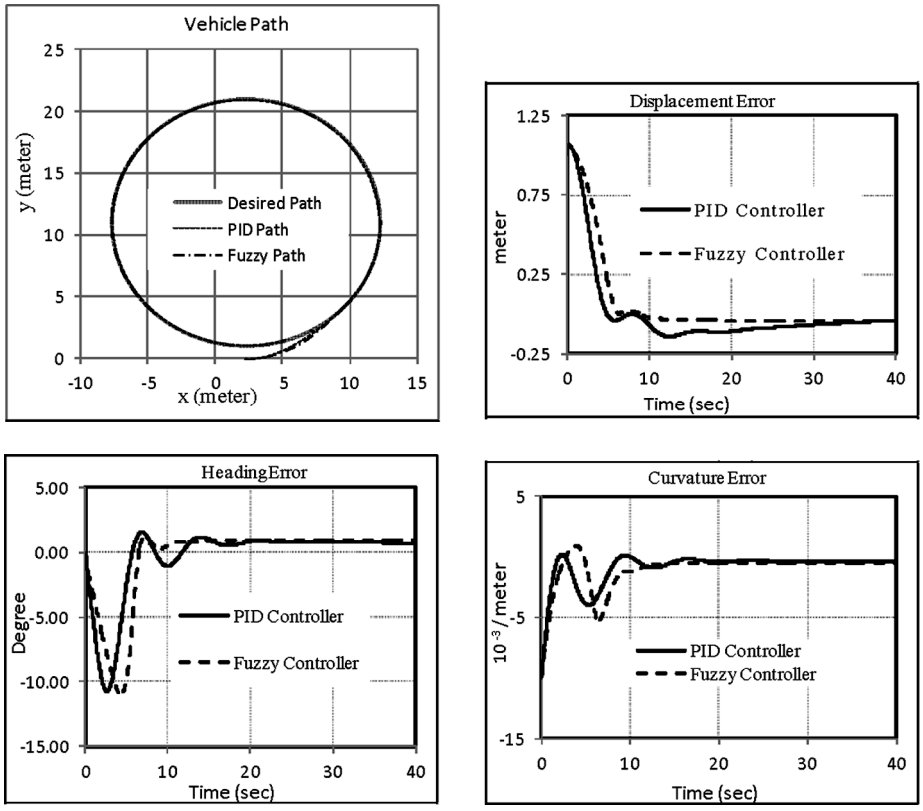

Figure 13 shows the simulation results for the LWL navigating a predefined path consisting of variable segments, this path is generated using Reeds and Shepp (1990) path optimising methodology. This methodology works based on specifying the start point, the end point, and the minumu turning radous. This variable segments path consists of three events; turn left, drive straight and turn right. Any complex path can be analysed to be formed of these events (Reeds and Shepp, 1990). Again, both controllers, the fuzzy logic and the PID, have reasonable rising and settling times, also the PID controller brought the vehicle faster closer to desired path, however it took longer time to settle the machine on the desired path.

Figure 13 An articulated vehicle navigating a predefined segmented path

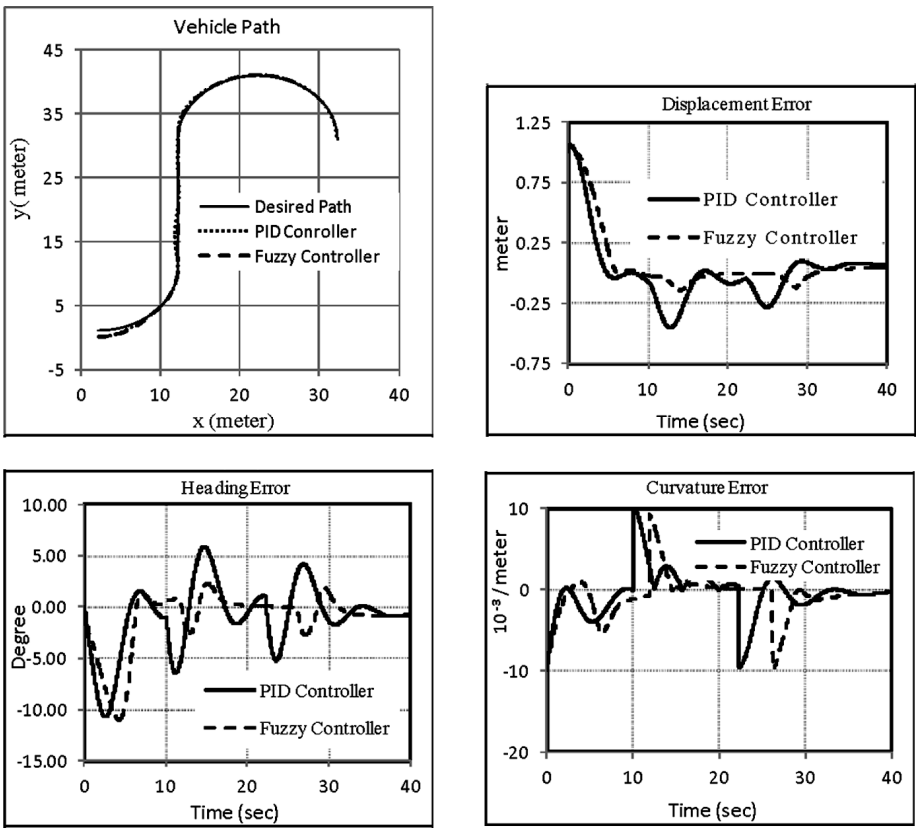

These results show that using multibody mechanical systems modelling along with computational dynamic solution methods to model the vehicle allows merging different system together enhances the accuracy of the simulation.

Describing the path and the controller model independently from the machine's technical parameters gives the possibility to change whole path characteristics without compromising the relevance and validity of the simulation. In this work, there was no need to change controllers or machine parameters when different paths were simulated.

References

Alshaer, B., Darabesh, T. and Alhanouti, M. (2013) 'Path planning. modeling and simulation of an autonomous articulated heavy construction machine performing a loading cycle', *Applied Mathematical Modeling*, Vol. 37, No. 7, pp.5315–5325.

Altafini, C. (1999) 'Path-tracking criterion for an LHD articulated vehicle', *The International Journal of Robotics Research*, Vol. 18, No. 5, pp.435–441.

Corke, P. and Ridley, P. (2001) 'Steering kinematics for a center-articulated mobile robot', *IEEE Transactions on Robotics and Automation*, Vol. 17, No. 2, pp.215–218.

Debeleac, C. (2009) 'Nonlinear approaches on dynamics of multibody mechanical systems with advanced computing tools', *WSEAS International Conference on Automation & Information (CAI'09)*, 23–25 March, Prague, Czech Republic, pp.100–104.

DeSantis, R. (1997) 'Modeling and path-tracking for a load-haul-dump mining vehicle', *Journal of Dynamic Systems, Measurement, and Control*, Vol. 119, No. 1, pp.40–47.

Divelbiss, A. and Wen, J. (1997) 'A path space approach to nonholonomic motion planning in the presence of obstacles', *IEEE Transactions on Robotics and Automation*, No. 13, pp.443–452.

Dragt, B., Camisani-Calzolari, F. and Craig, I. (2005) 'Modeling the dynamics of a load-haul dump vehicle', *Proceedings of the 16th IFAC World Congress*, Czech Republic, pp.1389-1389.

Ferrara, A. and Magnani, L. (2004) 'Hybrid variable structure path tracking control of articulated vehicles', *Proceeding of the 2004 American Control Conference*, 30 June–2 July, Boston, Massachusetts, Vol. 3, pp.2777–2782.

Filla, R. (2005) 'An event-driven operator model for dynamic simulation of construction machinery', *The Ninth Scandinavian International Conference on Fluid Power*, 1–3 June, Linköping, Sweden, pp.1–6.

Ghabcheloo, R. and Hyvönen, M. (2009) 'Modeling and motion control of an articulated-frame-steering hydraulic mobile machine', *17th Mediterranean Conference on Control & Automation, Makedonia Palace*, 24–26 June, Thessaloniki, Greece, pp.92–97.

Ghabcheloo, R., Hyvönen, M., Uusisalo, J., Karhu, O., Järä, J. and Huhtala, K. (2009) 'Autonomous motion control of a wheel loader', *2nd Annual Dynamic Systems and Control Conference*, 12–14 October, Hollywood, CA, USA, pp.427–434.

Ho, M., Chan, P., Rad, A. and Mak, C. (2003) 'Truck backing up neural network controller optimized by genetic algorithm', *Proceedings IEEE Conference on Evolutionary Computation*, No. 2, pp.944–950.

Kalyoncu, M. (2007) 'Mathematical modelling and dynamic response of a multistraight-line path tracing flexible robot manipulator with rotating-prismatic joint', *Appl. Math. Model.*, Vol. 32, April, pp.1087–1098.

Koyachi, N. and Sarata, S. (2009) 'Unmanned loading operation by autonomous wheel loader', *ICROS-SICE International Joint Conference*, Fukuoka International Congress Center, 18–21 August, Japan, pp.2221–2225.

Lamiraux, F., Bonnafous, D. and Geem, C. (2003) 'Path optimization for nonholonomic systems: application to reactive obstacle avoidance and path planning', *Springer Tracts in Advanced Robotics*, No. 4, pp.1–18.

Norris, W.R., Zhang, Q. and Sreenivas, R.S. (2006) 'Rule-base reduction for a fuzzy human operator performance model', *Applied Engineering in Agriculture*, Vol. 22, No. 4, pp.611–618, American Society of Agricultural and Biological Engineers ISSN 0883-8542.

Pacejka, H. (2002) *Tire and Vehicle Dynamics*, 2nd ed., Butterworth-Heinemann, USA.

Polotski, V. and Hemami, A. (1997) 'Control of articulated vehicle for mining applications: modeling and laboratory experiments', *Proceedings of the 1997 EEE International Conference on Control Applications*, 5–7 October, Hartford, CT, pp.318–323.

Reeds, J. and Shepp, L. (1990) 'Optimal paths for a car that goes both forwards and backwards', *Pacific Journal of Mathematics*, Vol. 145, No. 2, pp.367–393.

Ridley, P. and Corke, P. (2001) 'Autonomous Control of an Underground Mining Vehicle', *Australian Conference on Robotics and Automation*, pp.26–31.

Sarata, S., Koyachi, N., Tubouchi, T., Osumi, H., Kurisu, M. and Sugawara, K. (2008) 'Development of autonomous system for loading operation by wheel loader', *International Symposium on Automation and Robotics in Construction*, pp.466–471.

Sarata, S., Weeramhaeng, Y. and Tsubouchi, T. (2005a) 'Planning of scooping position and approach path for loading operation by wheel loader', *International Symposium on Automation and Robotics in Construction ISARC*, 11–14 September, Ferrara, Italy, pp.1–6.

Sarata, S., Weeramhaeng, Y. and Tsubouchi, T. (2005b) 'Approach path generation to scooping position for wheel loader', *Proceeding IEEE International Conference on Robotics and Automation*, Barcelona, Spain, pp.1809–1814.

Sarata, S., Weeramhaeng, Y., Horiguchi, A. and Tsubouchi, T. (2006) 'V shape path generation for loading operation by wheel loader', *The 23rd International Symposium on Automation and Robotics in Construction. ISARC 2006*, pp.591–602.

Sasiadek, J.Z. and Lu, Y. (2005) 'Path tracking of an autonomous LHD articulated vehicle', *Proc. of 16-th IFAC World Congress*, July, Praha, Czech Republic, p.1390.

Yavin, Y. (2005) 'Modeling the motion of an underground mining vehicle', *Mathematical and Computer Modeling*, Vol. 42, Nos. 9–10, pp.1123–1130.

Yossawee, W., Tsubouchi, T., Sarata, S. and Yuta, S. (2002) 'Path generation for articulated steering type vehicle using symmetrical clothoid', *Proc. IEEE International Conf. on Industrial Technology*, No. 1, pp.187–192.